Improved detectability in low signaltonoise ratio magnetic resonance images by means of a phasecorrected real reconstruction

M. A. Bernstein, David M. Thomasson, and William H. Perman

Articles you may be interested in

Automatic computation of signal-to-noise ratio for magnetic resonances images
AIP Conf. Proc. **1494**, 124 (2012); 10.1063/1.4764619

Exploiting differences in underwater acoustic signal and noise distributions to improve signal detection in low signal-to-noise ratio
J. Acoust. Soc. Am. **132**, 1941 (2012); 10.1121/1.4755145

Coded penumbral imaging for improvements of signal-to-noise ratio
Rev. Sci. Instrum. **75**, 4017 (2004); 10.1063/1.1787901

An unbiased signaltonoise ratio measure for magnetic resonance images
Med. Phys. **20**, 1077 (1993); 10.1118/1.597004

Lesion detection and signal–to–noise ratio in CT images
Med. Phys. **8**, 13 (1981); 10.1118/1.594903

Improved detectability in low signal-to-noise ratio magnetic resonance images by means of a phase-corrected real reconstruction

M. A. Bernstein[a], David M. Thomasson, and William H. Perman[b]
Department of Medical Physics and Radiology University of Wisconsin, Madison, Wisconsin 53706

We show that for magnetic resonance (MR) images with signal-to-noise ratio (SNR) < 2 it is advantageous to use a phase-corrected real reconstruction, rather than the more usual magnitude reconstruction. We discuss the results of the phase correction algorithm used to experimentally verify the result. We supplement the existing literature by presenting closed form expressions (in an MR context) for the probability distribution and first moments of the signal resulting from a magnitude reconstruction.

I. INTRODUCTION

Standard magnetic resonance (MR) imaging employs two-channel quadrature detection, so that the raw data consist of an array of complex numbers. In the most common reconstruction technique, a complex discrete 2D-Fourier transform (FT) is performed on the raw data, often with suitable windowing. Two resulting images can be displayed, the "real" image, whose pixel values are equal to the real part of the complex 2D-FT of the data, and the analogous "imaginary" image. Additionally a "magnitude" image can be formed by taking the square root of the sum of the squares of the real and imaginary images on a pixel-by-pixel basis. When the Hermitian property of the raw data is satisfied, the imaginary part of the reconstructed image will have zero signal.[1] While the imaginary image is not expected to contain signal in most cases, it will invariably contain noise. Therefore the real image has noise properties different from the magnitude image. In this note we demonstrate the effect of these noise properties on detectability, and give some theoretical background for the results. We discuss a phase correction algorithm used for the experiment. The primary application of this technique is reconstruction of images with low SNR such as those acquired from alternative nuclei such as sodium and fluorine.

II. PHASE CORRECTION ALGORITHM

Many commercial MR scanners only display the magnitude image, despite its disadvantages. Magnitude images are used because real images have artifacts, due to signal occurring in both the real and imaginary channels, unless special procedures are followed. Typical reasons for this mixing of signal include (1) noncentering of the echo in the data acquisition window due to pulse timing errors or eddy currents, (2) phase encoding gradient steps which are not symmetrically centered about zero, (3) phase shifts arising from hardware sources such as the bandpass filters, and (4) patient-to-patient variations in coil loading which change the coil impedance, thereby causing phase shifts.

Recently we presented an automatic postprocessing algorithm for phase correction of the real image. The details of this algorithm are given in Ref. 2. The basic algorithm is to solve a least-squares problem for a set of phasing coefficients, where the quantity to be minimized is the imaginary part of the phase corrected image. The advantage of this method is that arbitrarily high-order phase correction can be applied to both the readout and phase-encoded directions separately. Since our algorithm requires starting guesses for the low-order phase correction parameters, we found that it complements the linear correction method of Ahn and Cho[3] quite well. At present our technique is a research tool due to its relatively slow phasing times (2–4 min image on a Data General MV 4000 without an array processor, 30 s to 1 min with an AP.) Also the method does not work for gradient recalled echoes of objects containing a mixture of chemical shifts (e.g., fat water), unless the echo time is carefully selected so that the phase shift between the different chemical species is a multiple of pi. For the present detectability study, however, the method was useful. The more accurate (quartic) phase correction reduced a possible systematic error from the experiment: degradation of the real phased-corrected image due to leakage into imaginary channel.

The scans presented were performed on a General Electric Signa MR system. All scans were obtained with a slice thickness of 10 mm, a 24 cm field of view, and unless otherwise noted, a single Hahn echo with TE = 25 ms. Fig. 1(a) shows the unphased real image of a human volunteer. Note the banding artifact. Figure 1(b) shows the phase corrected real image as processed by the algorithm. To appreciate the advantage of a higher-order correction, Figures 1(c) and 1(d) display the imaginary image which should only contain noise. Figure 1(c) shows the result of only zero and first-order corrections in both the readout and phase encoded directions. Figure 1(d) shows the advantage of zero through fourth-order corrections.

III. DETECTABILITY EXPERIMENT

Figure 2(a) is a magnitude image of a detectability phantom consisting of eight rows of Lucite inserts with diameters ranging from 1.6 to 12.7 mm in a 154 mM saline solution. Figure 2(b) shows the same raw data processed to give the phased real image. Note that the detectability is not significantly changed, although the noise texture differs. The SNR in Fig. 2(b) is 2.15. Figures 2(c) and 2(d) show the same phantom imaged with a SNR of 0.80. At this lower SNR there is a difference in detectability between the magnitude and phase corrected real reconstruction. Figure 3 shows how
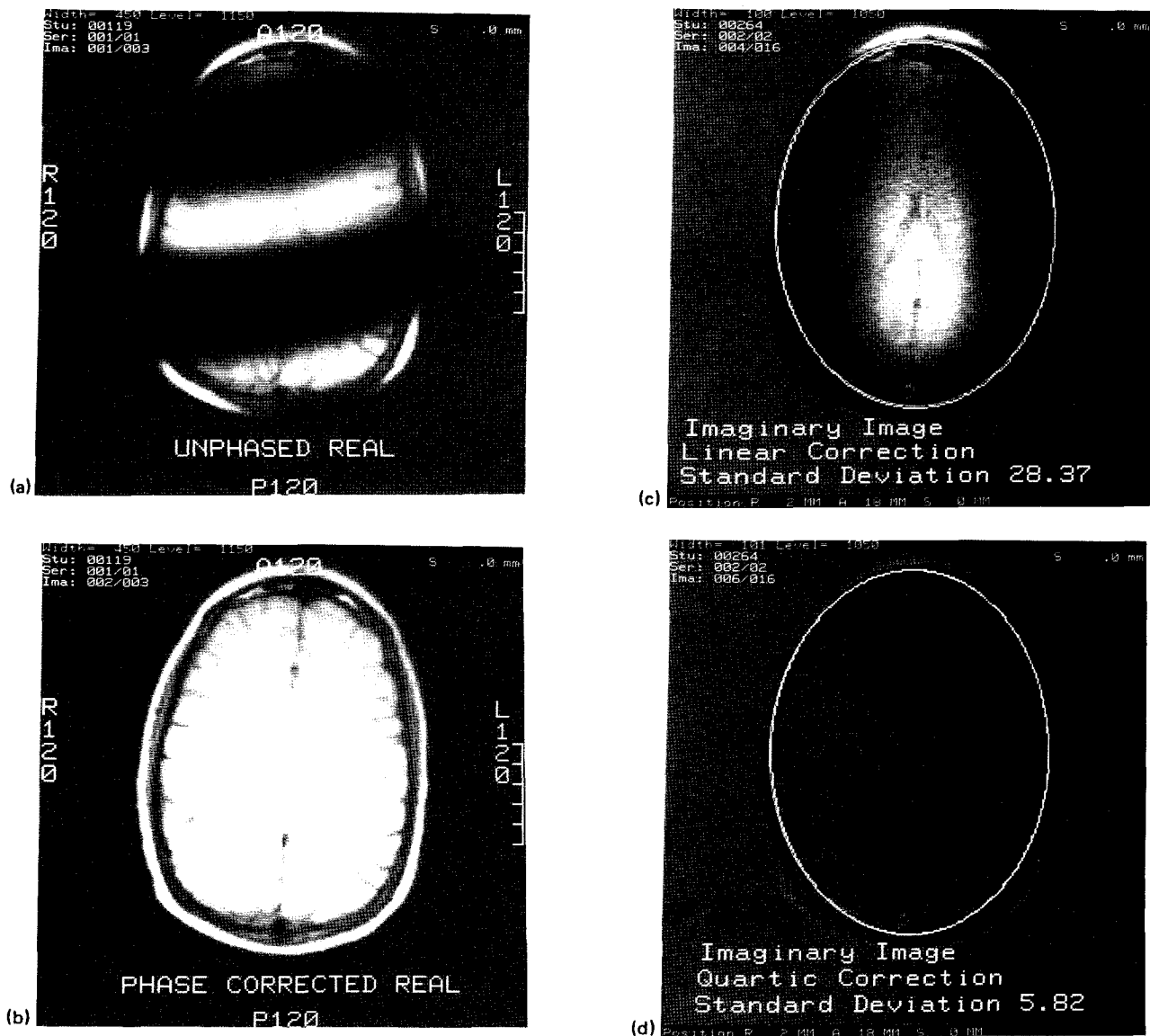
FIG. 1. (a) Unphased real image of a human volunteer. (b) Phase corrected real image reconstructed from the sme raw data using the algorithm of Ref. 2. (c) Imaginary image after linear phase correction. The standard deviation applies to the oval region of interest indicated. (d) Imaginary image after 4th order phase correction.

the detectability[4] depends on SNR for the two different reconstruction methods. In agreement with Fig. 2, the difference in detectability increases as the SNR decreases. Above SNR = 2 little advantage is gained with the phase-corrected reconstruction. The next section presents a theoretical development is support of this result.

IV. NOISE DISTRIBUTION IN REAL AND MAGNITUDE IMAGES

The noise character in a magnitude image differs from the noise character in the corresponding phased real image. The difference is significant for regions of the image with SNR near zero, but rapidly becomes negligible as the SNR is increased. This subject has been discussed in an MR context by Henkelman,[5] and by Edelstein et al,[6] and in a nuclear medicine context by Holden.[7] In a Communications Systems con-

text this effect has been derived by Rice,[8] and is discussed in undergraduate texts, for example Taub and Schilling.[9] Here we supplement those treatments, by developing closed-form expressions in an MR context for the probability density function of interest, and its first two moments. We adopt the model and notation used in Ref. 5. Let the MR signal in a pixel in the real phase image be A, and the independent Gaussian noise in the real and imaginary channels each have variance σ^2. Then the normalized joint probability distribution $P(x,y;A,\sigma)$ for pixel intensities in the real and imaginary images is given by

$$P(x,y;A,\sigma) = P(x;A,\sigma) \, P(y;A.\sigma),$$

(1)

where

$$P(x;A,\sigma) = \frac{\exp\{-(x-A)^2/2\sigma^2\}}{(2\pi\sigma^2)^{1/2}},$$
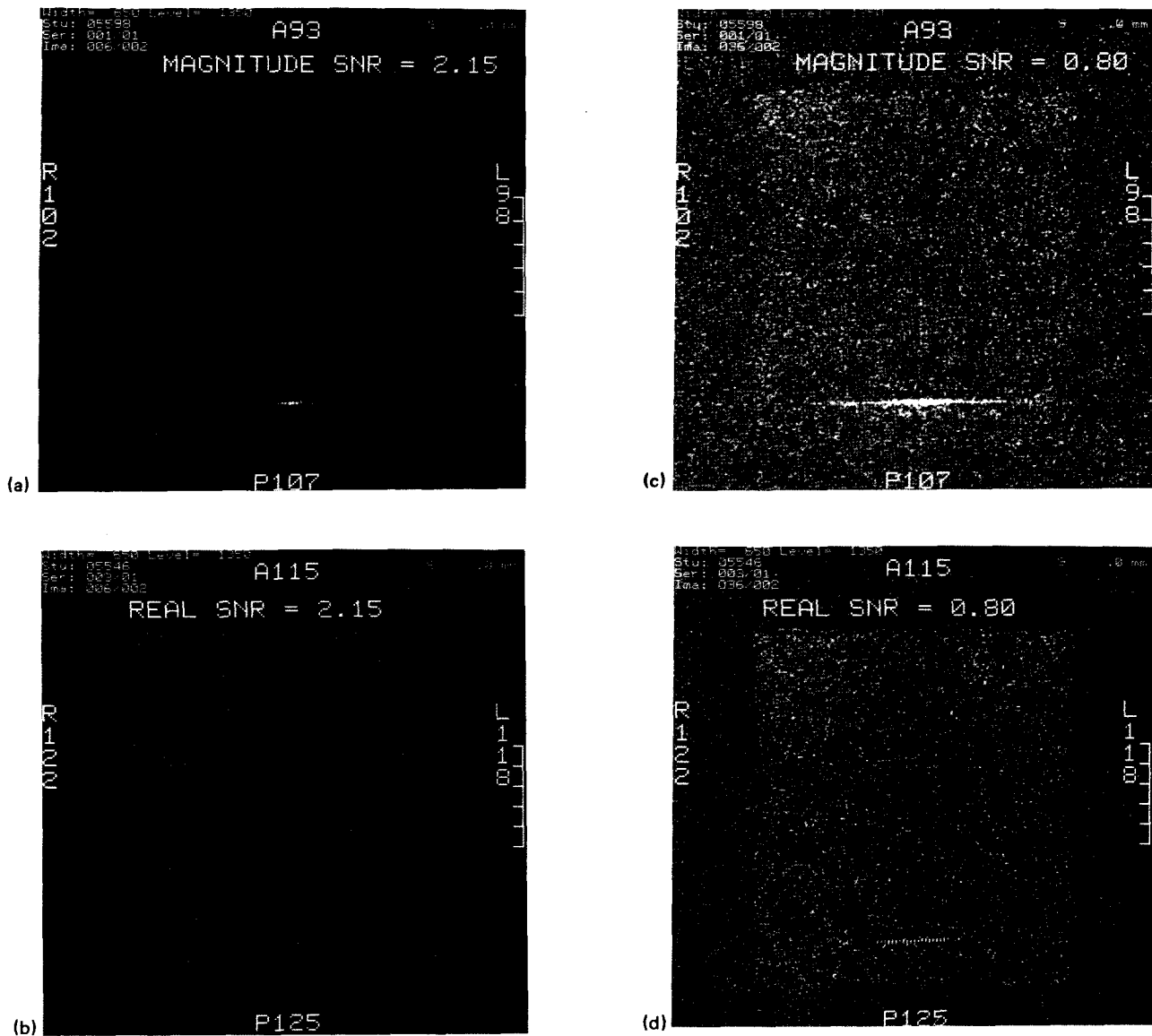
(2a)

(a)

(b)

(c)

(d)

FIG. 2. (a) Magnitude image of a detectability phantom. (b) Phase corrected real image reconstructed from the same data. (c) Magnitude image from lower SNR data. (d) Phase corrected real image reconstructed from the same data as (c). Note the improved detectability.

$$P(y;A,\sigma) = \frac{\exp\{-y^2/2\sigma^2\}}{(2\pi\sigma^2)^{1/2}}. \qquad (2b)$$

The probability distribution for the pixel intensity M in the magnitude image can be obtained by reexpressing $P(x,y;A,\sigma)$ in terms of the polar coordinates

$$x = M\cos\theta, \, y = M\sin\theta. \qquad (3a)$$

Multiplying $P(x,y;A,\sigma)$ by the Jacobian determinant

$$\frac{\partial(x,y)}{\partial(M,\theta)} = M \qquad (3b)$$

and then integrating over the angular variable θ yields the result

$$P(M;A,\sigma) = \frac{M\exp\{-(M^2+A^2)/2\sigma^2\}I_0(MA/\sigma^2)}{\sigma^2}, \qquad (4)$$

where I_0 is the zero-order modified Bessel function.[10] The asymptotic expansion[10] of I_0 for large values of its arguments gives

$$P(M;A,\sigma) \sim \left[\frac{M}{A}\right]^{1/2} \frac{\exp\{-(M-A)^2/2\sigma^2\}}{(2\pi\sigma^2)^{1/2}}, \quad A/\sigma \text{ large}. \qquad (5)$$

Equation (5) differs from the probability distribution for the pixel intensity in the real phased image, $P(x;A,\sigma)$, only by the multiplicative factor $(M/A)^{1/2}$. The exponential in Eq. (5) insures that $P(M;A,\sigma)$ is sharply peaked at $M\approx A$, where the multiplicative factor $(M/A)^{1/2}\approx 1$. Therefore in this high-SNR limit, $P(M;A,\sigma)$ approximates $P(x;A,\sigma)$. In Fig. 4, $P(M;A,\sigma)$ and $P(x;A,\sigma)$ are plotted for SNR $= A/\sigma$ of 0,1, and 3. Note the rapid convergence of $P(M;A,\sigma)$ toward $P(x;A,\sigma)$ as the SNR increases. Figure 4(d) shows an experimental histogram of pixel values in the background of
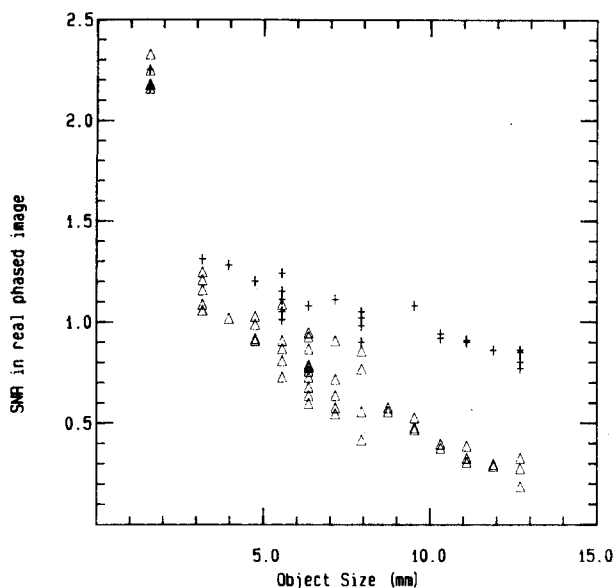
FIG. 3. Detectability plotted vs SNR. The triangles correspond to phase corrected real images, and the + 's correspond to magnitude images.

magnitude and real images, displaying functional dependence similar to that of Fig. 4(a).

The mean M_{avg} (A,σ) and standard deviation M_{SD} (A,σ) of the distribution given by Eq. (4) are of interest. The second moment of the signal in the magnitude image can be obtained from Eq. (4):

$$\langle M^2 \rangle = 2\sigma^2 + A^2, \tag{6}$$

in agreement with Ref. 5. Therefore the standard deviation is related to the mean M_{avg} (A,σ) through the relation

$$M_{SD}(A,\sigma) = \left[2\sigma^2 + A^2 - M_{avg}^2(A,\sigma) \right]^{1/2}. \tag{7}$$

Results of a numerical calculation for M_{avg} (A,σ) are presented in Ref. 5. We note here that M_{avg} (A,σ) has a closed-form expression[8]:

$$M_{avg}(A,\sigma) = \sigma(\pi/2)^{1/2}e^{-(A^2/4\sigma^2)}$$

$$\times \{(1 + A^2/2\sigma^2)I_0(A^2/4\sigma^2) + (A^2/2\sigma^2)I_1(A^2/4\sigma^2)\}, \tag{8}$$

where I_1 is the first-order modified Bessel function. Asymptotic expansions[10] of the Bessel functions show that
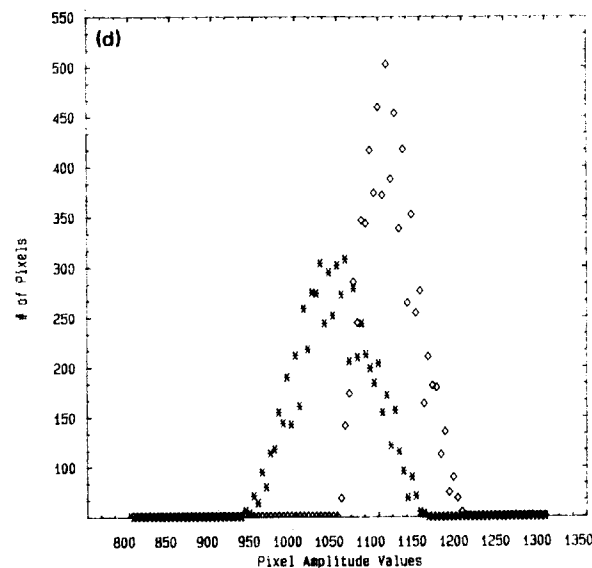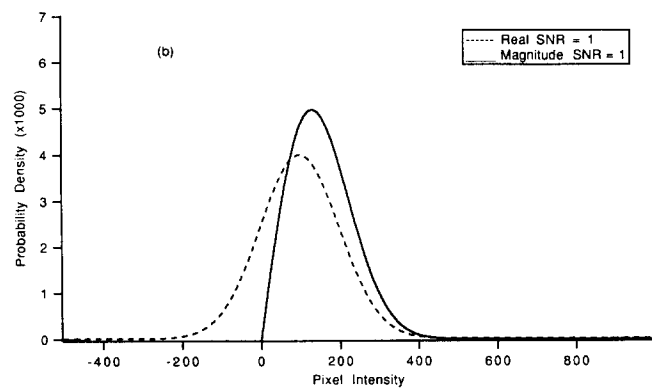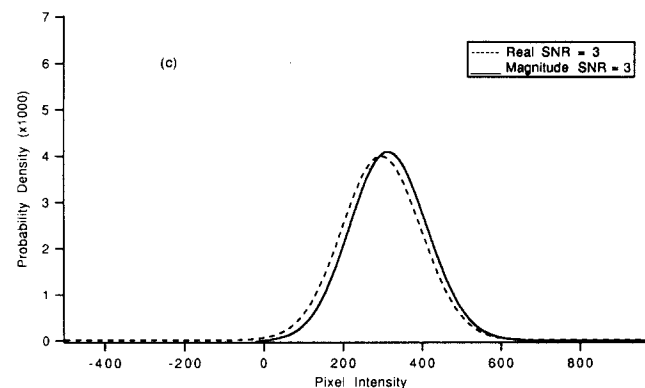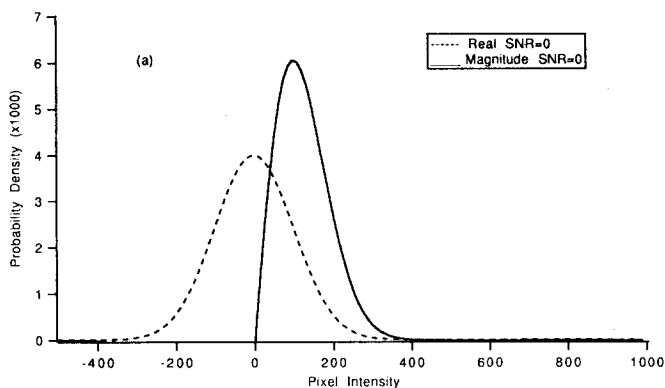

FIG. 4. (a–c) Probability density plotted vs pixel intensity for the distributions given by Eqs. (2a) and (4) for three values of A/σ. The dashed lines correspond to Eq. (2a), and solid lines to Eq. (4). (d) Experimental demonstration of the zero SNR distribution plotted in (a).

$$M_{avg}(A,\sigma) \sim A(1 + \frac{\sigma^2}{2A^2} + \frac{\sigma^4}{8A^4} + ...), \quad A/\sigma \text{ large,}$$

$$(9)$$

so that

$$M_{SD}^2(A,\sigma) \sim \sigma^2(1 - \sigma^2/2A^2 + ...), A/\sigma \text{ large.} \quad (10)$$

$M_{SD}(A,\sigma)$ is a measure of the width of the distribution for the pixel intensity in the magnitude image. The value of $M_{SD}(A = 0,\sigma) = 0.655\sigma$. As A increases $M_{SD}(A,\sigma)$ increases, asymptotically approaching the value σ as illustrated by Eq. (10). This dependence is also plotted in Ref. 5. Since the value of $M_{SD}(A,\sigma)$ is bounded by the inequality $M_{SD}(A,\sigma) \leq \sigma$, one might believe that the magnitude image is "less noisy" than the phased real image. Nevertheless, for interpretation of low SNR regions in images, the real phased image is superior to the magnitude image as shown by Fig. 2. The primary reason for this is illustrated by Figs. 5(a) and 5(b). Figure 5(a) shows the real distributions for SNR = 0
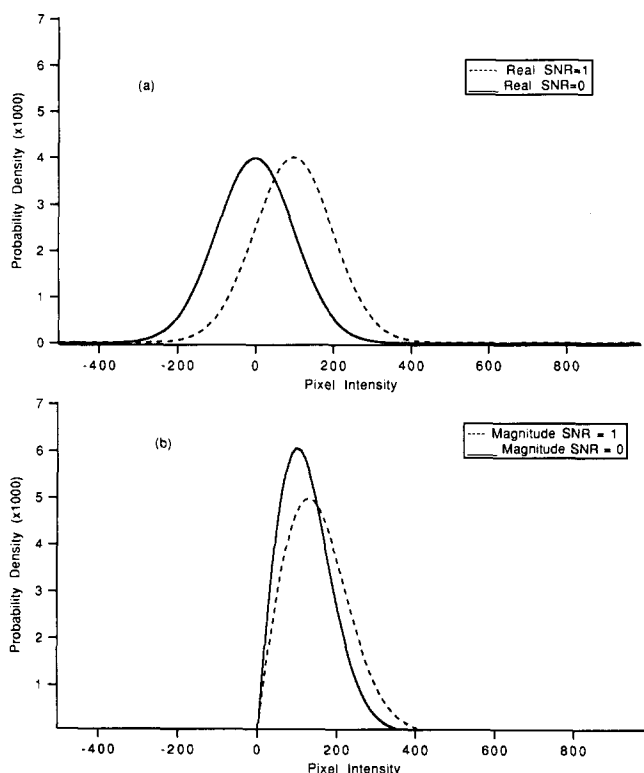

FIG. 5. (a) Probability density plotted vs pixel intensity for $A/\sigma = 0$ and 1 real distributions. (b) Magnitude distributions for the same cases.

and 1 together, and similarly Fig. 5(b) shows the magnitude distributions. Comparison of these plots indicates the distribution for $P(M;A,\sigma)$ is not symmetric about its mean, but instead has a "tail" extending to values of $M \geq M_{SD}(A,\sigma)$. The noise from the background of the image, represented by the tail from the zero-SNR distribution $P(M;A = 0,\sigma)$ [Fig. 5(b)] can interfere with the detection of an object which produces a low-SNR signal in the image.

V. CONCLUSION

Detectability in low SNR regions of MR images is improved by the use of the phased real reconstruction. We have presented experimental and theoretical evidence for this result.

ACKNOWLEDGMENTS

[a] Current address: W826, General Electric Medical Systems, P.O. Box 414, Milwaukee, Wisconsin 53201
[b] Current address: Mallinckrodt Institute of Radiology Washington University, St. Louis, Missouri 63110

[1] K. F. King and P. R. Moran, "A Unified description of NMR imaging, data collection strategies, and reconstruction", Med. Phys. 11, 1 (1984).
[2] M. A. Bernstein and W. H. Perman, "Least Squares Algorithm for Phasing of MR images", Abstract #801, SMRM sixth Annual Meeting, New York, 1987).
[3] C. B. Ahn and Z. H. Cho, IEEE Trans. on Med. Imag. M16, 32 (1987).
[4] G. Cohen and F. A. DiBianca, "The use of contrast-detail-dose evaluation of image quality in a CT scanner," J. Comput. Assis. Tomography 3, 189 (1979).
[5] R. M. Henkelman,"Measurements of signal intensities in the presence of noise in MR images.", Med. Phys. 12, 232 (1985).
[6] W. A. Edelstein, P. A. Bottomley, and L. M. Pfeifer, Med. Phys. 11, 180 (1984).
[7] J. E. Holden, J. R. Halama, and B. H. Hasegawa, "Propagation of stochastic pixel noise into magnitude and phase values in the Fourier analysis of digital images", Phys. Med. Bio. 31, 383 (1986).
[8] S. O. Rice, "Mathematical Analysis of Random Noise", Bell System Tech. J. 23, 282 (1944). (Reprinted by N. Wax, Selected Papers on Noise and Stochastic Process", Dover Publications 1954 QA273W3).
[9] H. Taub and D. L. Schilling Principles of Communications Systems, (McGraw Hill, New York, 1971), p. 287.
[10] Handbook of Mathematical Functions, edited by M. Abromowitz and A. Stegun (Dover, New York, 1972), Chaps. 9 and 11.